MESSENGER Observations of Reconnection in Mercury's Near-Magnetotail Under Strong IMF Forcing

Jun Zhong[1,2], Lou-Chuang Lee[3,4], James A. Slavin[5], Hui Zhang[1,2], Yong Wei[1,2]

[1]Key Laboratory of Earth and Planetary Physics, Institute of Geology and Geophysics, Chinese Academy of Sciences, Beijing, China

[2]Heilongjiang Mohe National Observatory of Geophysics, Institute of Geology and Geophysics, Chinese Academy of Sciences, Beijing, China

[3]Institute of Earth Sciences, Academia Sinica, Taipei, Taiwan

[4]State Key Laboratory of Lunar and Planetary Sciences, Macau University of Science and Technology, Macau, China

[5]Department of Climate and Space Sciences and Engineering, University of Michigan, Ann Arbor, Michigan, USA

Corresponding author: Jun Zhong (j.zhong@mail.iggcas.ac.cn)

Key Points:

- First statistical survey of near-tail reconnection events under strong IMF forcing at Mercury.
- More reconnection events were observed on the duskside and they were located farther down the tail than on the dawnside.
- Multiple flux rope events formed in Hall region were observed most frequently on the dawnside.

This is the author manuscript accepted for publication and has undergone full peer review but has not been through the copyediting, typesetting, pagination and proofreading process, which may lead to differences between this version and the Version of Record. Please cite this article as doi: 10.1029/2022JA031134.

Abstract

The MESSENGER spacecraft typically crossed Mercury's magnetotail current sheet relatively close to the planet, i.e. less than 2.5 R_M (planet radius; 2440 km). Magnetometer measurements are used to detect active reconnection events by identifying the quadrupole Hall magnetic field signatures that form about X-lines. Statistical analyses of the 51 active reconnection events detected in this manner indicate that they occur most frequently on the duskside and typically at a mean altitude greater than 1.5 R_M. In contrast, the dawnside events occur at altitudes of ~1 R_M. In addition, a higher recurrence rate of flux ropes formed in the Hall region was observed on the dawnside. Applying the Kan-Lee solar wind - magnetosphere coupling function confirmed that these near-tail reconnection events at Mercury are observed under strong forcing by the interplanetary magnetic field. We further propose that the reconnection-driven nightside magnetosphere–planet interaction is characterized by a pronounced dawn-dusk asymmetry and may significantly influence the near-Mercury space environment.

1 Introduction

Magnetic reconnection is a universal fundamental plasma process that alters the topology of magnetic fields and converts magnetic energy into plasma energy (e.g., *Lee and Lee*, 2020). Similar to Earth, reconnection occurs at Mercury's dayside magnetopause and in the nightside magnetotail current sheet, allowing the input of solar wind energy and driving the global magnetic flux and plasma circulation in the magnetosphere (e.g., *Slavin et al.*, 2021). The strong solar wind driving, weak intrinsic magnetic field (*Anderson et al.*, 2011), and lack of significant ionosphere, combined with relatively small scale of the magnetosphere (e.g., *Winslow et al.*, 2013; *Zhong et al.*, 2015), may result in reconnection at Mercury that differs from that at Earth. Especially, Mercury's magnetosphere is much more responsive to the interplanetary magnetic field (IMF) direction and is more dominated by the effects of reconnection than that of Earth or of the other magnetized planets (*Slavin et al.*, 2009).

At Earth, tail reconnection, which is widely considered to be responsible for triggering substorm onset (e.g., *Angelopoulos et al.*, 2008), is preferably initiated on the duskside (e.g., *Eastwood et al.*, 2010; *Nagai et al.*, 2015). Geotail flux rope (FR) and Cluster traveling compression region (TCR) observations show this asymmetry at Earth very clearly (*Slavin et al.*,

2005). They found that FR and TCR events in the near-nightside plasma sheet and lobes, respectively, occur more frequently, and have larger cross-sections and higher bulk speeds on the duskside as compared to the dawnside of Earth's magnetotail. These FR and TCR observations favoring reconnection onset and peak intensity on the duskside of the magnetotail are consistent with numerous studies of the cross-tail current sheet showing it to be thinner on the duskside, on average, with increased asymmetry favoring the onset of reconnection just prior to substorms (*Artemyev et al.*, 2016).

Mercury's tail current sheet, on average, is also thinner on the duskside than on the dawnside (*Poh et al.*, 2017a; *Rong et al.*, 2018). As thin current sheets are closely associated with the onset of magnetic reconnection, it is expected that the occurrence of reconnection would also be more frequent on the duskside than on the dawnside. Nevertheless, reconnection-related magnetic structures or phenomena, e.g., dipolarizations, flux ropes, and energetic electron injections, are more typically observed by the MESSENGER spacecraft on the dawnside than on the duskside (e.g., *Lindsay et al.*, 2016; *Sun et al.*, 2016; *Smith et al.*, 2017; *Dewey et al.*, 2020). Some of these magnetotail asymmetries at Mercury have been reproduced by simulations of reconnection and magnetic flux transport that consider the east-west spatial extents of reconnection X-lines, i.e. 10's ion inertial lengths (d_i) in Mercury's magnetotail, which has a diameter estimated to be a few 10's *di* (*Chen et al.*, 2019; *Dong et al.*, 2019; *Liu et al.*, 2019). As first proposed by Lu et al. (*Lu et al.*, 2018), the reconnection flows sunward from finite length X-lines that form in the duskside cross-tail current sheet and the magnetic flux that they transport will tend to follow the electron flow and be diverted eastward or toward the dawnside. At Mercury, where the tail width is comparable to the east-west length of the reconnection X-lines, this eastward diversion of magnetic flux transport may result in duskside reconnection driving strong convection, dipolarization fronts, flux ropes, and magnetic flux transport on the dawnside as opposed to the duskside (*Liu et al.*, 2019).

A comparative analysis of tail flux rope polarities for three MESSENGER flybys under different IMF conditions implied that the near-Mercury neutral line locations can be significantly changed (*Slavin et al.*, 2012). During MESSENGER's three equatorial flybys, the location of reconnection X-lines in Mercury's tail were observed to be at a downstream distance of X_{MSM} ~ – 1.8 to – 2.8 R_M when the IMF was southward and substorm-like tail magnetic flux loading and unloading events were observed (*Slavin et al.*, 2012). However, the average location of the tail

X-lines was later inferred to be at a downstream distance of $X_{MSM} \sim -3\ R_M$ using current sheet crossings and flux rope observations during the 4-year orbital phase (*Poh et al.*, 2017b; *Smith et al.*, 2018).

The distance at which reconnection events form in the Earth's magnetotail is shown to decrease as the rate of energy input at the magnetopause increases and increase as the energy transfer rate, or power, decreases (*Nagai et al.*, 2005). On a few occasions, tail reconnection can even occur near the geosynchronous orbit driven by the enhanced solar wind dynamic pressure and southward magnetic field (e.g., *Angelopoulos et al.*, 2020). Under strong solar wind driving, Mercury's tail reconnection is expected to be closer to the planet and thus detectable by the MESSENGER in the near-tail. Such an extremely driven reconnection in the near-Mercury magnetotail was first reported by *Zhong et al.* (2018). Their observations revealed the rapid and impulsive nature of the exceedingly driven reconnection signatures during a period of ~35 s, during which the average reconnection rate can reach 0.2. In another active reconnection event, driven by an ICME, multiple X-line reconnections were dominant in the tail current sheet, which drove Mercury's magnetospheric dynamics globally and continuously produced flux ropes (*Sun et al.*, 2020a; *Zhong et al.*, 2020a). These observations suggest that reconnection and energy dissipation in Mercury's near-tail can be continuous in the planetward of MESSENGER's < 2.5 R_M tail traversals during its ~ 4-year orbital phase.

Here, we identified reconnection events in Mercury's magnetotail current sheet throughout the entire MESSENGER mission. A pronounced dawn-dusk asymmetry in the near-Mercury tail reconnection is revealed. Similar to Earth, more reconnection events were observed on the duskside. On the dawnside, the reconnection events were observed closer to the planet and produced flux ropes at higher rates and in greater total numbers. These near-Mercury reconnection events are closely related to the strong southward interplanetary magnetic fields upstream of Mercury. Hence, they may represent a directly driven response to the IMF rather than a pattern of tail loading followed by a spontaneous or triggered releases of stored magnetic energy from the lobes as sometimes observed (*Slavin et al.*, 2010; *Imber and Slavin*, 2017). Our new findings are important for better understanding and physical modeling of Mercury's small magnetosphere located in relative proximity to the Sun. For this reason our results may have applicability to the interaction of stellar winds with terrestrial-type exoplanets in tight orbits about their stars (*See et al.*, 2014).

2 Reconnection Events in Mercury's Magnetotail

2.1 Identification of Reconnection Events

A key signature for identifying active reconnection is the quadrupole Hall magnetic field structure, resulting from ion-electron decoupling in the ion diffusion region (*Sonnerup*, 1979). In the reconnection events during orbits 503 and 877 (*Zhong et al.*, 2018; *Zhong et al.*, 2020a), the MESSENGER south-to-north crossed the tail current sheet and observed a significant positive-to-negative bipolar feature in the out-of-plane magnetic field component B_M with overall negative B_N. Another key reconnection feature is the formation of multiple flux rope (FR) structures. FRs are commonly identified from magnetic field data, by the positive-to-negative (tailward moving) or negative-to-positive (planetward moving) polarity in B_N, coincident with the enhancements in B_M and/or total field $|\mathbf{B}|$. In two events, the observed FRs with positive-to-negative polarity in B_N suggest that these reconnection structures were moving tailward and passing the spacecraft sequentially. Both the quadrupole Hall magnetic field structures and FR signatures are consistent with that the spacecraft was located tailward of the reconnection region where multiple X-lines were initialized during the whole crossing, as the basic theoretical structure of quadrupole Hall magnetic field illustrated in Figure 1a and 1d. In a local tail current sheet coordinate system (LMN), L is directed along the reconnecting component of the magnetic field pointing planetward, M is along the guide field (X-line) direction pointing duskward, and N is the current sheet normal pointing northward. If the spacecraft cross the current sheet planetward of the X-lines, the magnetic field component B_N is expected to be positive, and the Hall magnetic field (in the B_M component) exhibits the same polarity as the reconnection field B_L (Figure 1b).

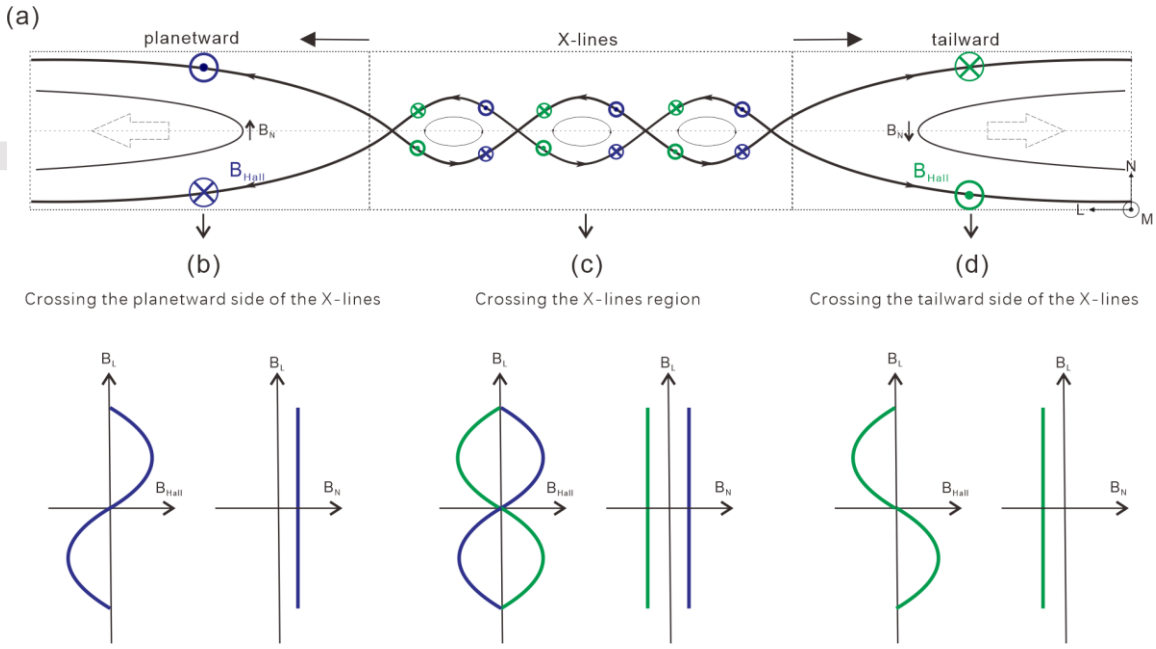

Figure 1. (a) The basic theoretical structure of the reconnection quadrupole Hall magnetic field in the local current sheet coordinate (LMN) system. (b)-(d) Predicted Hall magnetic field detected in the MN and LN planes when the spacecraft north-south crossing of reconnecting current sheet in three cases: (1) the planetward of the X-lines (Case 1), (2) X-lines region (Case 2), and (3) the tailward of the X-lines (Case 3).

These quadrupole Hall magnetic field patterns were used to search for near-Mercury's active reconnection events. Magnetic field data from the Magnetometer (MAG) (*Anderson et al.*, 2007), assisted by the ion flux data from the Fast Imaging Plasma Spectrometer (FIPS) (*Andrews et al.*, 2007), were used to identify the current sheet or plasma sheet crossings. We chose the solar wind-aberrated Mercury solar magnetospheric (MSM) coordinate, assuming the radial solar wind velocity 400 km/s, for analyses performed in this study. The LMN coordinates can be commonly well determined by the minimum variance analysis of the magnetic field (*Sonnerup and Scheible*, 1998). While in a few cases, the N direction may not be accurately obtained from variance analysis due to the insufficient separation between the intermediate and minimum eigenvalues. An alternate method for the normally expected magnetotail configurations to determine the N and M direction, i.e., $\mathbf{N} = \mathbf{L} \times (z_{MSM} \times \mathbf{L})$ and $\mathbf{M} = \mathbf{N} \times \mathbf{L}$, was performed well for Mercury, as adopted in the analysis of the reconnection event during orbit 877 (*Zhong et al.*, 2018). For most events, there is only a slight difference between the two methods, which does

not affect the identification of the Hall magnetic field. In this study, we present the results of the latter uniformly.

2.2 Reconnection Event During Orbit 3630

An overview of the MESSENGER observations of the tail current sheet crossing during orbit 3630 is shown in Figure 2a-e. The magnetic field data were rotated to the LMN coordinates. Relative to the aberrated MSM coordinate system, L = (0.98, −0.17, 0.15), M = (0.17, 0.99, 0), and N = (−0.14, 0.02, 0.99). During the main current sheet crossing, the negative-to-positive reversal in B_L indicates north–south crossing of the current sheet. The average B_N from 5-s smoothed data (gray traces) is negative throughout the crossing. The out-of-plane magnetic field component B_M shows an overall positive-to-negative bipolar signature, with a reversal at ~07:07:04 UT. The Hall magnetic field is also evident in the magnetic field hodograms (Figure 2f, 2g), as predicted by the theory in Figure 1d. The Hall magnetic field structure is slightly distorted, probably due to the presence of a weak negative guide field during the reconnection.

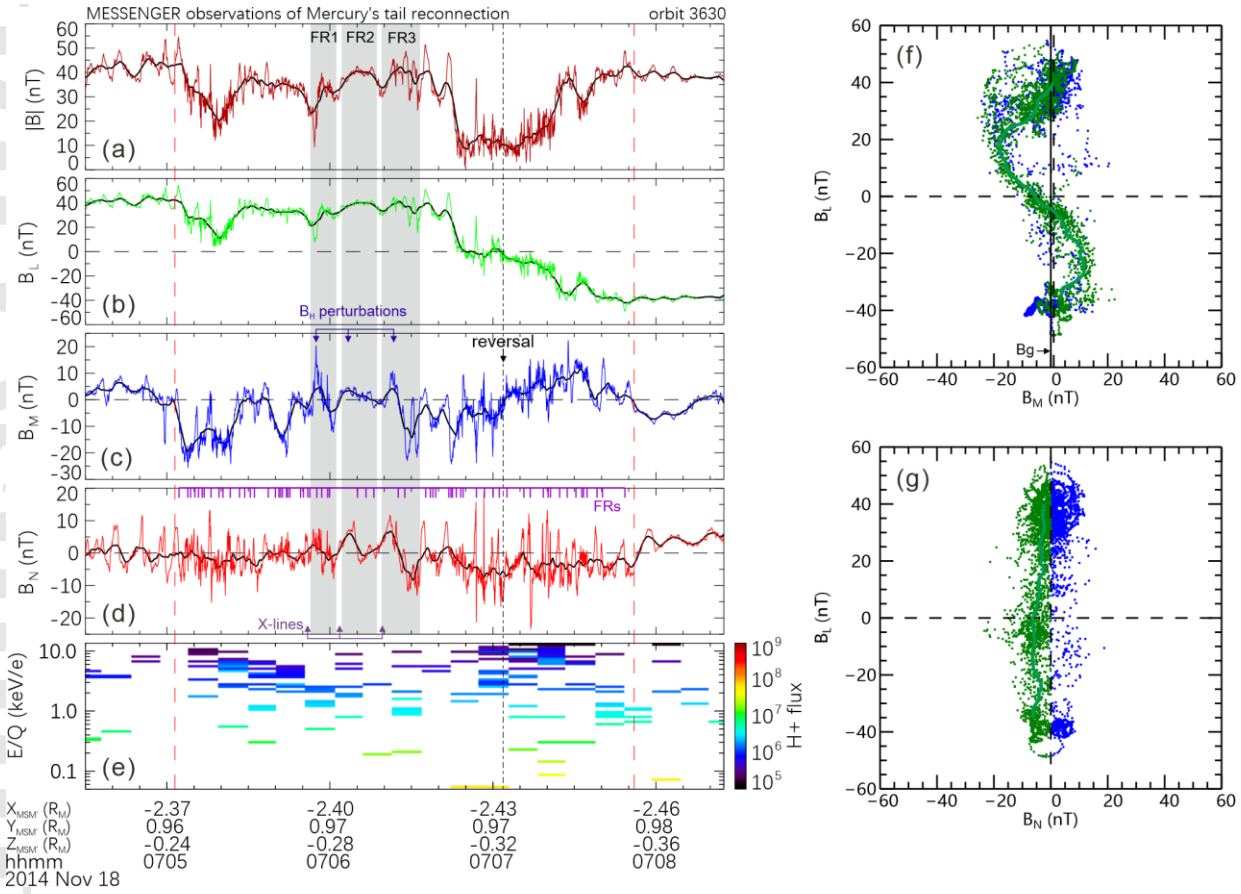

Figure 2. MESSENGER observations of magnetic reconnection in Mercury's magnetotail during orbit 3630. (a)-(d) Magnetic field magnitude and its three components in the LMN coordinates. (e) Spectrogram of the ion differential energy flux (cm^{-2} sr^{-1} s^{-1} keV^{-1}). Three long-duration FRs, labeled FR1–3, were identified from the 5 s smoothed magnetic field data (gray traces). The sequential crossing of X-lines, Hall magnetic field perturbations are marked by purple and blue arrows, respectively. The FRs identified from the high resolution data are marked in (d). (f) and (g) Magnetic field hodograms in the B_L-B_M and B_L-B_N planes, respectively, plotted through the time interval between two vertical dashed lines (identified as the Hall region). Blue (green) denotes positive (negative) B_N data. The thick trajectories are the median values with 5 nT bin-smoothed magnetic field hodograms.

The large perturbations of the Hall magnetic field and the formation of FRs suggest that the evolution of the reconnection was highly unstable. From high-resolution magnetic field data sampled at 20 s^{-1}, a large number of small-scale FRs with timescales of ~1 s can be identified (red arrows). The typical timescales of ~1 s may correspond to the ion-scale structures. The

positive-to-negative polarities in B_N are indicative of tailward-moving FR structures. The interaction and coalescence of multiple FRs into larger ones are a common reconnection signature in Mercury's space, not only in the tail current sheet but also at the magnetopause, as comprehensively analyzed by *Zhong et al*. (2020a; 2020b). The key observational feature is that the long-duration bipolar B_N (smoothed) structure consisted of multiple successive short-duration bipolar variations. Three long-duration FRs, labeled FR1–3, were clearly identified from the smoothed data before the spacecraft close to the current sheet center. The negative-to-positive reversals of B_N just before FRs FR1–3 and subsequent positive perturbations of the Hall magnetic field in the FRs leading part indicate that the spacecraft passed multiple tailward moving X-lines, as denoted by the purple arrows in Figure 2(d). These tailward moving reconnection structures further confirm that the X-lines were initialized in the planetward of the spacecraft.

2.3 Reconnection Event During Orbit 3378

An overview of the MESSENGER observations of the tail current sheet crossing during orbit 3378 is shown in Figure 3a-e. The magnetic field data were rotated to the LMN coordinates. Relative to the aberrated MSM coordinate system, L = (0.96, −0.27, 0.11), M = (0.27, 0.96, 0), and N = (−0.10, 0.03, 0.99). The spacecraft north–south crossed the main current sheet at ~ 02:39:00 UT, indicated by the negative-to-positive reversal in B_L. In this event, the guide field $B_g \approx 6$ nT. The magnetic Hall field, $B_H = (B_M - B_g)$, shows a positive-to-negative reversal at the current sheet center. The average B_N (smoothed data) is overall positive throughout the crossing. These magnetic field signatures suggest that the spacecraft crossed the planetward of the X-line during the current sheet crossing. The Hall magnetic field is also evident in the magnetic field hodograms (Figure 3f, 3g), as predicted by the theory in Figure 1b.

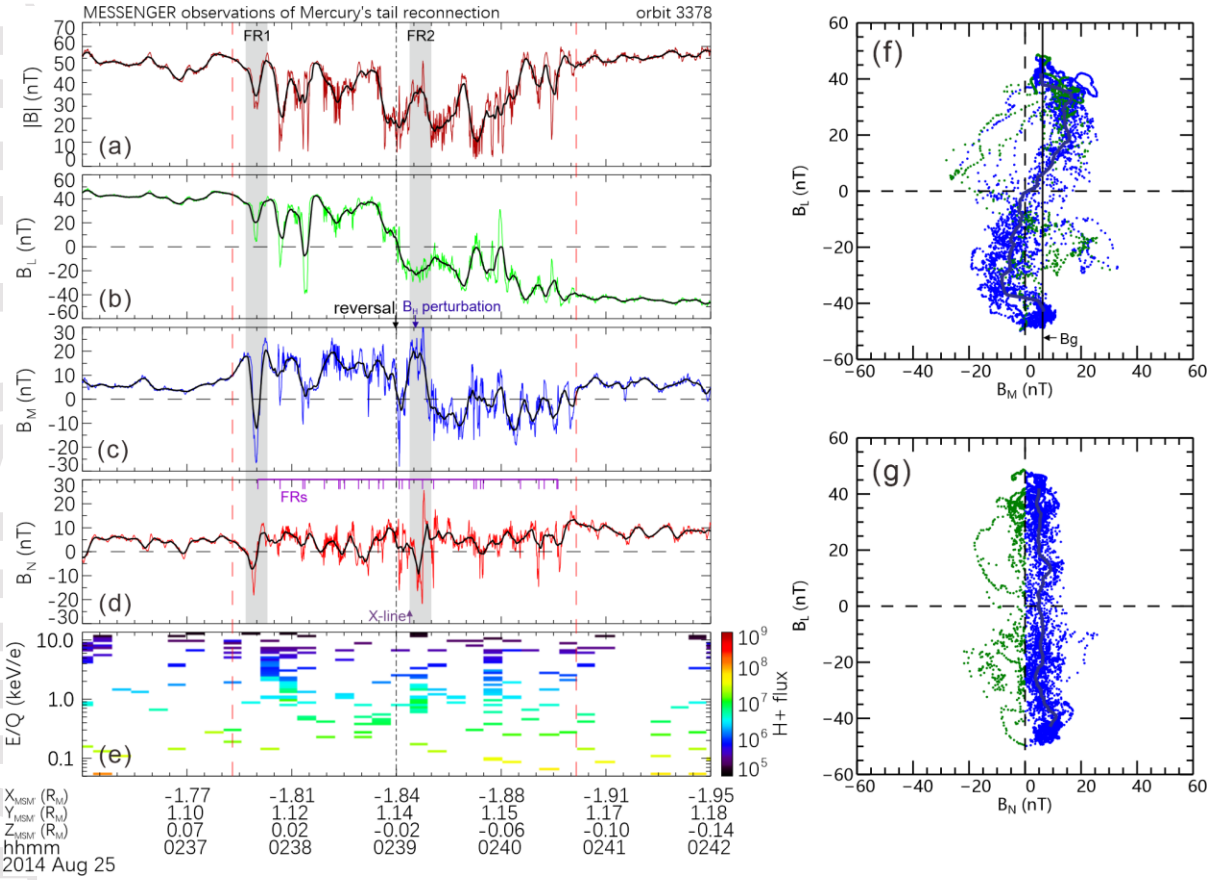

Figure 3. MESSENGER observations of magnetic reconnection in Mercury's magnetotail during orbit 3378. The layout is the same as in Figure 2.

The passage of the X-line and consequent long-duration or large-scale FR were also observed in this event. After the MESSENGER crossed the current sheet into the southern hemisphere, the B_N dropped and became negative at ~02:39:08 UT (purple arrow in Figure 3d). The reversal of B_N from positive to negative corresponds to the reversal of B_H from negative to positive, indicating that a planetward moving X-line passes through the spacecraft. Following the X-line is a large-scale FR (FR2). The negative-to-positive polarity suggests a planetward moving FR structure. Such large-scale planetward moving FR (FR1) was also encountered before the current sheet crossing, when the spacecraft was located in the northern hemisphere. These planetward moving reconnection structures further confirm that the X-lines were initialized in the tailward of the spacecraft.

2.4 Reconnection Event During Orbit 2809

When the MESSENGER crossing X-lines region closely enough, the full quadrupole Hall magnetic field structures may be detected by a single spacecraft. An example is shown in Figure 4. The magnetic field data were rotated to the LMN coordinates. Relative to the aberrated MSM coordinate system, L = (0.97, 0.23, 0.03), M = (−0.23, 0.97, 0), and N = (−0.03, −0.01, 1.00). The spacecraft crossed the tail current sheet from north ($B_L > 0$) to south ($B_L < 0$) close to the planet at ~ 1.76 R_M downstream. In this event, the guide field $B_g \approx 4$ nT. The clear multiple B_N reversals indicate that the spacecraft was passed by X-lines or O-lines. The duration of positive and negative B_N is almost equal, which makes X- or O-lines not well identifiable. The B_N and ($B_M - B_g$) have the same sign in the northern hemisphere and opposite signs in the southern hemisphere. Each B_N reversal corresponds to a reversal in B_M. These observations are consistent with the quadrupole Hall magnetic field patterns. The signatures in the magnetic field hodograms (Figure 4f, 4g) show a combination of the former two cases. The presence of such hodograms is most probably because the MESSENGER crossed the X-lines region sufficiently and the reconnection occurred under the rapidly evolving process in Mercury's magnetotail.

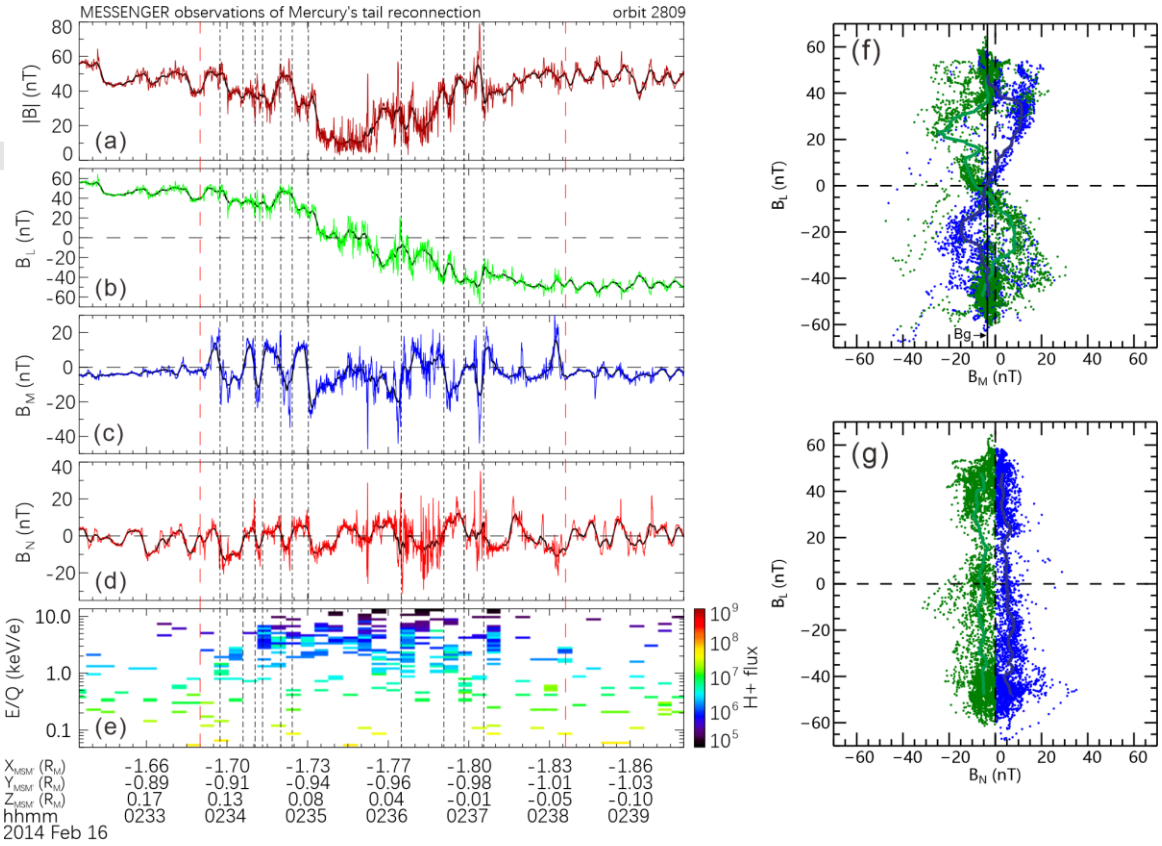

Figure 4. MESSENGER observations of magnetic reconnection in Mercury's magnetotail during orbit 2809. The layout is the same as in Figure 2.

A close-up view of multiple FRs observations during 02:36:00-02:37:20 UT is shown in Figure 5. At least 32 FRs can be clearly identified during the 80-s interval. Some clustering FRs may interact and merge into larger ones; a typical example is marked in Figure 5 (gray bar). Both positive-to-negative (tailward moving) and negative-to-positive (planetward moving) bipolar B_N signatures are observed. If the spacecraft is passed by a single X-line, the motion of FR structures is expected to be away from the X-line. However, some of FRs are observed moving towards the detected X-line, as indicated by the case of the positive-to-negative (negative-to-positive) B_N polarity within the positive (negative) B_N region. Two typical examples are marked by arrows in Figure 5c. A natural explanation is that another X-line occurred simultaneously nearby. These FR observations further suggest that the spacecraft was sufficiently close to the X-lines region where reconnection was triggered.

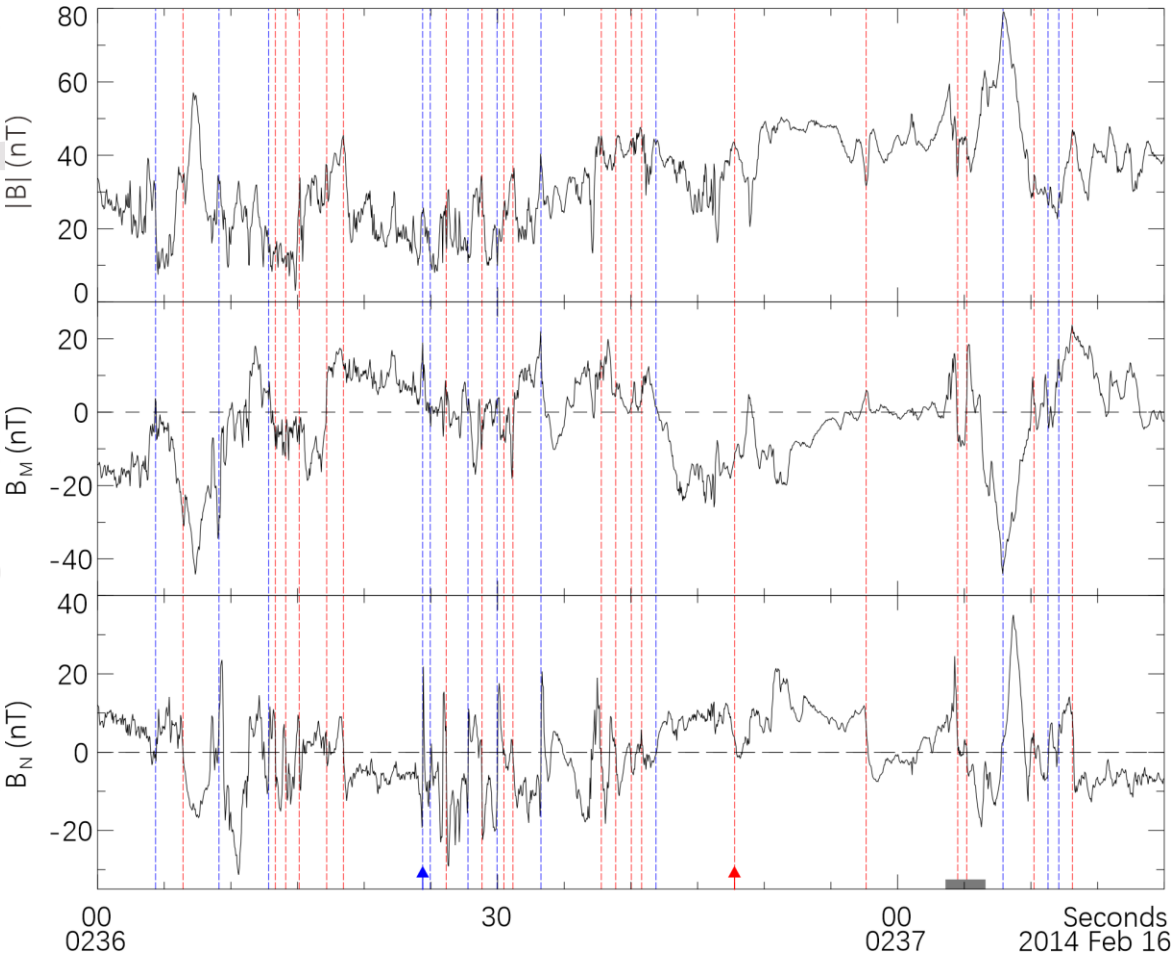

Figure 5. Close-up view of multiple FR observations. From top to bottom, magnetic field magnitude, B_M and B_N. Vertical blue and red dashed lines are identified planetward (negative-to-positive polarity) and tailward (positive-to-negative polarity) moving FRs, respectively. The blue and red arrows mark two typical examples of FRs moving toward an X-line. The gray bar marks an example of multiple small-scale FRs merging into a large one.

3 Statistical Results

We surveyed 4 years of MESSENGER data including 4084 orbits, from March 2011 to April 2015. A total of 51 reconnection events (Supporting information, , including orbits 877 and 503) were visually identified with clear Hall magnetic field signatures that showed consistency with the prediction theory (Figure 1). Using quadrupole Hall magnetic field patterns to identify the reconnection events requires that the reconnection remain continuous or active during the

current sheet crossing and be close enough to the spacecraft. During the majority of near-planet tail crossings, especially with dense and thick plasma sheets (*Zhao et al.*, 2020), Hall magnetic fields were not observed. This imply that the reconnection, if existing, is commonly intermittent or the normal location of X-lines is far downstream from the coverage of the MESSENGER.

According to the observed quadrupole Hall magnetic field, we categorized the reconnection events into (1) crossing the planetward side of the X-lines (Figure 1b, Case 1), (2) crossing of X-lines region (Figure 1c, Case 2), and (3) crossing the tailward side of the X-lines (Figure 1d, Case 3). A few reconnection events observed with the Hall magnetic field in three quadrupoles are classified into Case 2. The three categories have 27, 19, and 5 events, respectively.

3.1 Dawn-dusk Asymmetry: Reconnection Sites and Flux Rope Formation

The spatial distribution of the reconnection events in the magnetic equator plane of the aberrated MSM coordinate is shown in Figure 6a. These reconnection events occur beyond 1.5 R_M downstream of the planet in the region of Y'= −1.5 to 1.5 R_M, or magnetic local time (MLT) 21 to 03 h (Figure 6b). There are 30 and 21 events on the duskside and dawnside, respectively, with a maximum occurrence corresponding to the premidnight region (23 to 00 MLT). Notably, the MESSENGER tail equator crossings during the whole orbital mission were evenly distributed around midnight (gray dots in Figure 6a). The greater number of events on the duskside indicates a higher occurrence rate of near-planet tail reconnection. An alternative explanation for this asymmetric reconnection location is that the dawn-dusk width of the reconnection site is probably below 3 R_M (1 R_M corresponds to ~10-30 proton inertial scales), with its center in the premidnight region.

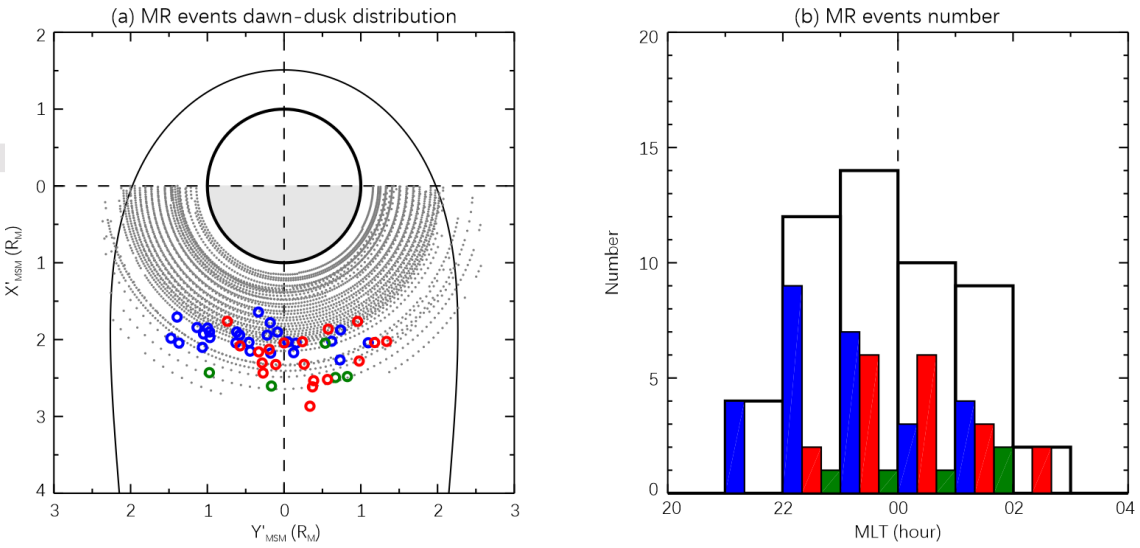

Figure 6. Spatial distribution of near-Mercury reconnection events observed by MESSENGER. (a) Location of events in the aberrated MSM X'-Y' plane. The solid curve represents the average magnetopause from the three-dimensional model (*Zhong et al.*, 2015). Blue, red, and green denote the events with crossing the planetward side of the X-lines (Case 1), crossing of X-lines region (Case 2), and crossing the tailward side of the X-lines (Case 3), respectively. The background gray dots represent tail equator crossings during the whole orbital mission. (b) Reconnection events occurrence as a function of the MLT. (c) Total number of observed flux ropes (top) and occurrence rate (bottom) as a function of the MLT.

On the duskside, the majority of events are planetward crossings of the X-lines (Case 1, blue color), indicating that the reconnection sites on the duskside are typically beyond $X'_{MSM}= -2\ R_M$. However, on the dawnside, the events are mostly crossings of the X-lines region (Case 2, red color), or tailward crossings of the X-lines (Case 3, green color). These tailward crossing events are mostly observed far on the dawnside. These indicate that the reconnection site is closer to the planet on the dawnside than on the duskside.

The formation of multiple FR structures is common in these active reconnection events. The FRs with B_N bipolar amplitude greater than 8 nT observed in the Hall region were selected for statistical analyses. We calculated the FR occurrence rate for each event by (N-1)/(ΔT), where N is the total FR number and ΔT is the time separation from the first to the last FR. The occurrence rate of FRs for these active reconnection events ranges from 2 to 18 counts/min

(Figure 7a). For events in Case 1, the median value of the FR occurrence rate is ~ 4 counts/min, while, for events in Cases 2 and 3, FRs were more frequently detected, with an occurrence rate almost greater than 5 counts/min. Although the total Hall region observation time on the duskside (116 min) is longer than on the dawnside (108 min), the total number of detected FRs is more on the dawnside (Figure 7, top). The averaged recurrence rate of FRs is higher on the dawnside than on the duskside (Figure 7, bottom). The number and occurrence rate of FRs are maximum in the postmidnight region (00 to 01 MLT).

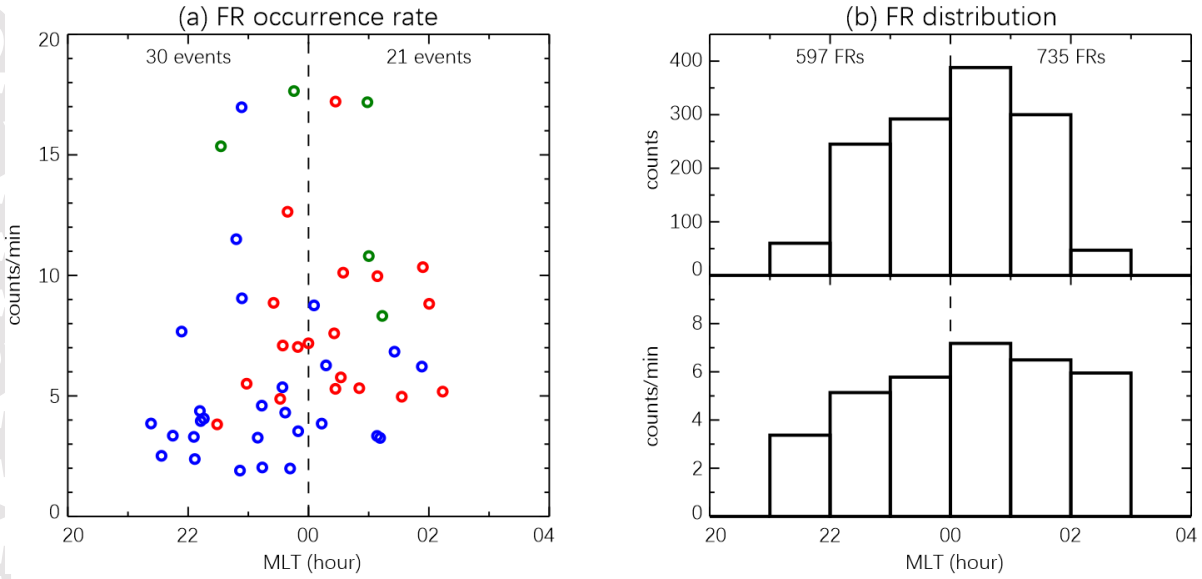

Figure 7. Statistical analysis of flux ropes in the Hall region. (a) FR occurrence rate for each reconnection event. (b) Total number of the observed FRs (top) and occurrence rate (bottom) as a function of the MLT.

The FR recurrence rate of these reconnection events is much higher than those detailed in previous statistical flux rope surveys (*Sun et al.*, 2016; *Smith et al.*, 2017). Applying an automated method, *Smith et al*. (2017) found that the majority of crossings did not feature any flux ropes within the 319 plasma sheet crossings, and the average peak rate of FRs is only 0.25 min^{-1} in post-midnight and only occasionally up to ~5 min^{-1} during active intervals. Since only cylindrical and force-free FRs were identified, their results may be underestimated. The much higher FR recurrence rate of our events is most likely due to the fact that the reconnection process remains active and occurs in the vicinity of the spacecraft.

3.2 Correlation with Strong IMF Forcing

The IMF measured just upstream of inbound and outbound bow shock is shown in Figure 8a. The observed reconnection events occurred under strong IMF conditions, with magnitudes predominantly above the average value (~24 nT). After being compressed by the bow shock, the perpendicular component (in the Y'-Z' plane) of the magnetic field could be further enhanced in the magnetosheath and draped outside the dayside magnetopause. Evidently, the observed reconnection events are associated with a strong perpendicular component of the magnetosheath field (B_{YZ} ~ 100 nT) and preferably occur under southward (B_Z < 0) conditions (Figure 8b).

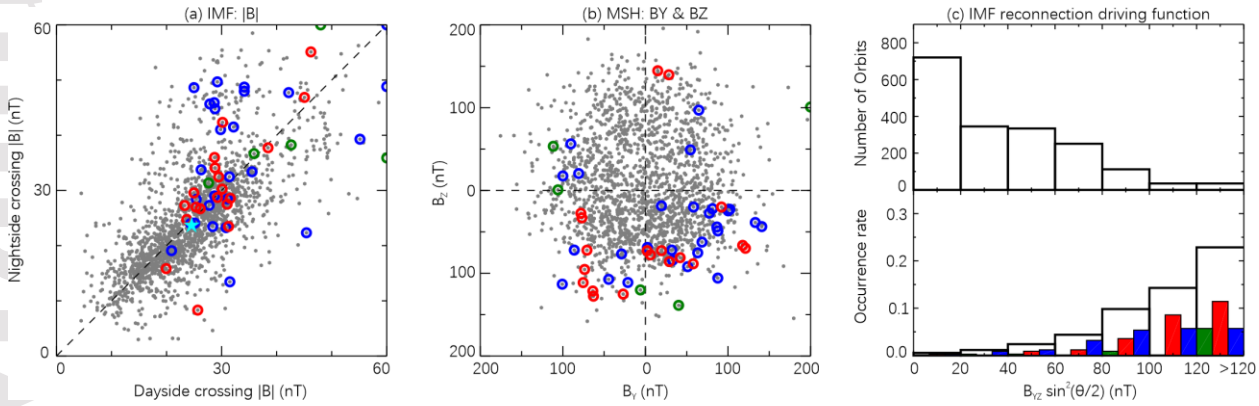

Figure 8. Statistical properties of IMF. (a) Magnitude of 1-min averaged IMF measured just outside of the dayside and nightside bow shock. (b) Magnetic fields, B_Y and B_Z, just outside the dayside magnetopause. (c) Histogram of the number of orbits crossing the equator region (top), and the occurrence rate of the observed reconnection events (bottom). Blue, red, and green denote events with crossing in the planetward of the X-lines (Case 1), X-lines region (Case 2), and the tailward of the X-lines (Case 3), respectively. Background gray dots show data for all tail equator crossings with $(X'_{MSM}{}^2+Y'_{MSM}{}^2)^{0.5} > 1.5\ R_M$ and MLT = 21-03 h. The cyan star denotes the average IMF value.

In theory, both the high magnetosheath magnetic field and the large magnetic shear across the magnetopause can increase the dayside reconnection rate (*Sonnerup*, 1974). The transportation of the magnetic flux from solar wind into the magnetosphere is closely related to the polar cap electric field, $E_{PC}=v_{SW}\cdot B_{YZ}\cdot\sin^2(\theta/2)$, where v_{SW} is the solar wind speed, perpendicular IMF $B_{YZ}=(B_Y^2+B_Z^2)^{0.5}$, and clock angle $\theta=\tan^{-1}(B_Y, B_Z)$ (*Kan and Lee*, 1979).

Because FIPS had an obstructed view of the solar wind beam by the sunshade, the upstream solar wind speed cannot be derived (*Raines et al.*, 2011). For the first order, we use the function, $F_{RD} = B_{YZ} \cdot \sin^2(\theta/2)$ to denote the reconnection level of the IMF driving, using the magnetic field measured in the magnetosheath just outside dayside magnetopause. In Figure 8c, the orbit number (top) and occurrence rate of the observed reconnection events (bottom) are plotted as a function of F_{RD}. It is clear that the near-Mercury reconnection occurrence rate strongly depends on F_{RD}. Eight-five percent of the reconnection occurrence rate is found under strong IMF forcing with $F_{RD} > 80$ nT.

4 Discussion

For the first time, we present a comprehensive analysis of reconnection in near-Mercury magnetotail observed by the MESSENGER spacecraft. Applying an IMF reconnection driving function, we found that the occurrence of these events is highly preferred under extreme IMF driving. On average, the dayside reconnection rate at Mercury would be greater than at Earth due to the low Alfvén Mach number conditions in the inner solar system (*Slavin and Holzer*, 1979), especially under the large magnetic shear angles and low plasma beta in the magnetosheath (*DiBraccio et al.*, 2013; *Sun et al.*, 2020b). Under extreme IMF driving, strong IMF reduces the upstream Alfvén Mach number and decreases the heating of the solar wind as it passes through the bow shock. The final result is a low beta magnetosheath with strong magnetic fields that frequently become comparable in magnitude to the field just inside the magnetopause (*Gershman et al.*, 2013). The reconnection rate of such "symmetric" reconnection, i.e., the intensity of the magnetic fields on either side of the magnetopause that become more symmetric, are found to be even faster (*Slavin et al.*, 2019).

The resulting intense dayside reconnection could quickly and continuously feed the magnetic flux into the tail. Majority of the tail reconnection events identified here were involving the lobe field rapid reconnection; see detailed analysis of orbit 503 as an example (*Zhong et al.*, 2018). The lower limit of the reconnection duration inferred from the average ion diffusion region (or Hall region) crossing time is 4.5 ±2.0 min, confirming that the tail reconnection can be continuous and stable over a prolonged period, considering the typical 3-4 min Dungey-cycle time scale (*Imber and Slavin*, 2017). A long-lasting balance between the magnetic flux transport

at the nightside and dayside is expected. These are consistent with direct driving by the IMF due to the short time response of Mercury's tiny magnetosphere (*Luhmann et al.*, 1998).

Statistical analyses of these continuous and quasi-stable reconnection events in the magnetotail revealed that reconnection occurs more frequently on the duskside, with spatial distribution centered in the premidnight region. In addition, the Hall magnetic field reversals suggested that reconnection is closer to the planet on the dawnside. Similar to the Earth, the thinner premidnight tail current sheet at Mercury (*Poh et al.*, 2017a; *Rong et al.*, 2018) likely triggers magnetic reconnection easily, resulting in more frequent reconnection on the duskside than on the dawnside. Conversely, planetary heavy ions, particularly Na^+, are enhanced on the duskside via mass loading from the dayside cusps (*Delcourt*, 2013; *Raines et al.*, 2013). These heavy ions on the duskside may reduce the upstream Alfvén speed, thereby reducing the reconnection rate and activity (e.g., *Shay and Swisdak*, 2004), compared with the dawnside. These may explain that more FRs in the ion diffusion region and their higher generation rate are observed on the dawnside. Herein, the spacecraft closer to the reconnection region on the dawnside may also affect the observational bias of the flux rope occurrence.

Notably, on the dawnside, the average location of the reconnection could be 2 R_M downstream or even closer to the planet, that is, ~2000 km above the nightside surface. The reconnection-produced energetic particles possibly have a direct impact on the planet surface. Considering the distance of the reconnection site, the particles reaching the planet's surface along the reconnected field lines are expected at a lower latitude on the dawnside than that on the duskside. Additionally, the weaker planetary surface magnetic field at the low latitude results in a larger loss cone angle; thus, the ratio of the precipitating particle flux would be larger on the dawnside. Note that the northward offset of Mercury's dipole field (*Anderson et al.*, 2011) also modifies the characteristics of the loss cone between the northern and southern hemispheres (*Korth et al.*, 2014; *Winslow et al.*, 2014). Conversely, such reconnection particle precipitation may occur more frequently on the duskside, where more reconnection events were observed. This asymmetry in the nightside reconnection-driven magnetosphere-planet interactions and its influence on the near-Mercury space environment can be analyzed via the simultaneous observations in both mid-tail and near-planet regions from the forthcoming dual spacecraft of the Bepi-Colombo mission (e.g., *Milillo et al.*, 2020; *Saito et al.*, 2021).

Acknowledgments

This work was supported by the B-type Strategic Priority Program of the Chinese Academy of Sciences (grant No. XDB41000000), the National Natural Science Foundation of China (41874198, 42174217, 41621004), and the Key Research Program of the Institute of Geology & Geophysics, CAS (Grant No. IGGCAS-201904 and IGGCAS-202102). L. C. Lee was supported by the Science and Technology Development Fund (FDCT) of Macau (0035/2018/AFJ) and the Ministry of Science and Technology, Taiwan (MOST 110-2111-M-002-017). J. A. Slavin acknowledges support from NASA grants 80NSSC18K1137, 80NSSC21M0364 and 80NSSC21K0052. MESSENGER data are available from the Planetary Data System (MAG: https://pds-ppi.igpp.ucla.edu/search/view/?f=yes&id=pds://PPI/mess-mag-calibrated/data/mso; FIPS: https://pds-ppi.igpp.ucla.edu/search/view/?f=yes&id=pds://PPI/mess-epps-fips-derived/data/espec). The list of the identified near-Mercury's tail reconnection events and flux ropes is available in the supporting information.

References

Anderson, B. J., M. H. Acuña, D. A. Lohr, J. Scheifele, A. Raval, H. Korth, and J. A. Slavin (2007), The Magnetometer instrument on MESSENGER, *Space Sci. Rev.*, *131*(1-4), 417-450, https://doi.org/10.1007/s11214-007-9246-7.

Anderson, B. J., C. L. Johnson, H. Korth, M. E. Purucker, R. M. Winslow, J. A. Slavin, S. C. Solomon, R. L. McNutt, J. M. Raines, and T. H. Zurbuchen (2011), The global magnetic field of Mercury from MESSENGER orbital observations, *Science*, *333*(6051), 1859-1862, https://doi.org/10.1126/science.1211001.

Andrews, G. B., et al. (2007), The Energetic Particle and Plasma Spectrometer instrument on the MESSENGER spacecraft, *Space Sci. Rev.*, *131*(1-4), 523-556, https://doi.org/10.1007/s11214-007-9272-5.

Angelopoulos, V., A. Artemyev, T. D. Phan, and Y. Miyashita (2020), Near-Earth magnetotail reconnection powers space storms, *Nature Physics*, *16*(3), 317-321, https://doi.org/10.1038/s41567-019-0749-4.

Angelopoulos, V., et al. (2008), Tail Reconnection Triggering Substorm Onset, *Science*, *321*(5891), 931-935, https://doi.org/doi:10.1126/science.1160495.

Artemyev, A. V., V. Angelopoulos, A. Runov, and A. A. Petrokovich (2016), Properties of current sheet thinning at x ∼− 10 to −12 RE, *Journal of Geophysical Research: Space Physics*, *121*(7), 6718-6731, https://doi.org/https://doi.org/10.1002/2016JA022779.

Chen, Y., G. Tóth, X. Jia, J. A. Slavin, W. Sun, S. Markidis, T. I. Gombosi, and J. M. Raines (2019), Studying Dawn-Dusk Asymmetries of Mercury's Magnetotail Using MHD-EPIC Simulations, *Journal of Geophysical Research: Space Physics*, *124*(11), 8954-8973, https://doi.org/10.1029/2019JA026840.

Delcourt, D. C. (2013), On the supply of heavy planetary material to the magnetotail of Mercury, *Ann. Geophys.*, *31*(10), 1673-1679, https://doi.org/10.5194/angeo-31-1673-2013.

Dewey, R. M., J. A. Slavin, J. M. Raines, A. R. Azari, and W. Sun (2020), MESSENGER Observations of Flow Braking and Flux Pileup of Dipolarizations in Mercury's Magnetotail: Evidence for Current Wedge Formation, *J. Geophys. Res. Space Physics*, *125*(9), e2020JA028112, https://doi.org/10.1029/2020ja028112.

DiBraccio, G. A., J. A. Slavin, S. A. Boardsen, B. J. Anderson, H. Korth, T. H. Zurbuchen, J. M. Raines, D. N. Baker, R. L. McNutt, and S. C. Solomon (2013), MESSENGER observations of magnetopause structure and dynamics at Mercury, *J. Geophys. Res. Space Physics*, *118*, 997-1008, https://doi.org/10.1002/jgra.50123.

Dong, C., L. Wang, A. Hakim, A. Bhattacharjee, J. A. Slavin, G. A. DiBraccio, and K. Germaschewski (2019), Global Ten-Moment Multifluid Simulations of the Solar Wind Interaction with Mercury: From the Planetary Conducting Core to the Dynamic Magnetosphere, *Geophysical Research Letters*, *46*(21), 11584-11596, https://doi.org/10.1029/2019gl083180.

Eastwood, J. P., M. A. Shay, T. D. Phan, and M. Øieroset (2010), Asymmetry of the Ion Diffusion Region Hall Electric and Magnetic Fields during Guide Field Reconnection: Observations and Comparison with Simulations, *Physical Review Letters*, *104*(20), 205001.

Gershman, D. J., J. A. Slavin, J. M. Raines, T. H. Zurbuchen, B. J. Anderson, H. Korth, D. N. Baker, and S. C. Solomon (2013), Magnetic flux pileup and plasma depletion in Mercury's subsolar magnetosheath, *J. Geophys. Res. Space Physics*, *118*(11), 2013JA019244, https://doi.org/10.1002/2013JA019244.

Imber, S. M., and J. A. Slavin (2017), MESSENGER Observations of Magnetotail Loading and Unloading: Implications for Substorms at Mercury, *J. Geophys. Res. Space Physics*, *122*(11), 11,402-411,412, https://doi.org/10.1002/2017JA024332.

Kan, J. R., and L. C. Lee (1979), Energy coupling function and solar wind-magnetosphere dynamo, *Geophysical Research Letters*, *6*(7), 577-580, https://doi.org/10.1029/GL006i007p00577.

Korth, H., B. J. Anderson, D. J. Gershman, J. M. Raines, J. A. Slavin, T. H. Zurbuchen, S. C. Solomon, and R. L. McNutt (2014), Plasma distribution in Mercury's magnetosphere derived from MESSENGER Magnetometer and Fast Imaging Plasma Spectrometer observations, *J. Geophys. Res. Space Physics*, *119*(4), 2013JA019567, https://doi.org/10.1002/2013JA019567.

Lee, L. C., and K. H. Lee (2020), Fluid and kinetic aspects of magnetic reconnection and some related magnetospheric phenomena, *Reviews of Modern Plasma Physics*, *4*(1), 9, https://doi.org/10.1007/s41614-020-00045-7.

Lindsay, S. T., M. K. James, E. J. Bunce, S. M. Imber, H. Korth, A. Martindale, and T. K. Yeoman (2016), MESSENGER X-ray observations of magnetosphere–surface interaction on the nightside of Mercury, *Planet. Space Sci.*, *125*, 72-79, https://doi.org/10.1016/j.pss.2016.03.005.

Liu, Y.-H., T. C. Li, M. Hesse, W. J. Sun, J. Liu, J. Burch, J. A. Slavin, and K. Huang (2019), Three-Dimensional Magnetic Reconnection With a Spatially Confined X-Line Extent: Implications for Dipolarizing Flux Bundles and the Dawn-Dusk Asymmetry, *Journal of Geophysical Research: Space Physics*, *124*(4), 2819-2830, https://doi.org/10.1029/2019JA026539.

Lu, S., P. L. Pritchett, V. Angelopoulos, and A. V. Artemyev (2018), Formation of Dawn-Dusk Asymmetry in Earth's Magnetotail Thin Current Sheet: A Three-Dimensional Particle-In-Cell

Simulation, *Journal of Geophysical Research: Space Physics*, *123*(4), 2801-2814, https://doi.org/https://doi.org/10.1002/2017JA025095.

Luhmann, J. G., C. T. Russell, and N. A. Tsyganenko (1998), Disturbances in Mercury's magnetosphere: Are the Mariner 10 “substorms” simply driven?, *J. Geophys. Res. Space Physics*, *103*(A5), 9113-9119, https://doi.org/10.1029/97JA03667.

Milillo, A., et al. (2020), Investigating Mercury’s Environment with the Two-Spacecraft BepiColombo Mission, *Space Sci. Rev.*, *216*(5), 93, https://doi.org/10.1007/s11214-020-00712-8.

Nagai, T., M. Fujimoto, R. Nakamura, W. Baumjohann, A. Ieda, I. Shinohara, S. Machida, Y. Saito, and T. Mukai (2005), Solar wind control of the radial distance of the magnetic reconnection site in the magnetotail, *Journal of Geophysical Research: Space Physics*, *110*(A9), https://doi.org/10.1029/2005JA011207.

Nagai, T., I. Shinohara, and S. Zenitani (2015), The dawn-dusk length of the X line in the near-Earth magnetotail: Geotail survey in 1994–2014, *Journal of Geophysical Research: Space Physics*, *120*(10), 8762-8773, https://doi.org/https://doi.org/10.1002/2015JA021606.

Poh, G., J. A. Slavin, X. Jia, J. M. Raines, S. M. Imber, W.-J. Sun, D. J. Gershman, G. A. DiBraccio, K. J. Genestreti, and A. W. Smith (2017a), Coupling between Mercury and its nightside magnetosphere: Cross-tail current sheet asymmetry and substorm current wedge formation, *J. Geophys. Res. Space Physics*, *122*(8), 8419-8433, https://doi.org/10.1002/2017JA024266.

Poh, G., J. A. Slavin, X. Jia, J. M. Raines, S. M. Imber, W.-J. Sun, D. J. Gershman, G. A. DiBraccio, K. J. Genestreti, and A. W. Smith (2017b), Mercury's cross-tail current sheet: Structure, X-line location and stress balance, *Geophy. Res. Lett.*, *44*(2), 678-686, https://doi.org/10.1002/2016GL071612.

Raines, J. M., et al. (2013), Distribution and compositional variations of plasma ions in Mercury's space environment: The first three Mercury years of MESSENGER observations, *Journal of Geophysical Research-Space Physics*, *118*(4), 1604-1619, https://doi.org/10.1029/2012ja018073.

Raines, J. M., J. A. Slavin, T. H. Zurbuchen, G. Gloeckler, B. J. Anderson, D. N. Baker, H. Korth, S. M. Krimigis, and R. L. McNutt Jr (2011), MESSENGER observations of the plasma environment near Mercury, *Planet. Space Sci.*, *59*(15), 2004-2015, https://doi.org/http://dx.doi.org/10.1016/j.pss.2011.02.004.

Rong, Z. J., Y. Ding, J. A. Slavin, J. Zhong, G. Poh, W. J. Sun, Y. Wei, L. H. Chai, W. X. Wan, and C. Shen (2018), The Magnetic Field Structure of Mercury's Magnetotail, *J. Geophy. Res. Space Physics*, *123*(1), 548-566, https://doi.org/10.1002/2017JA024923.

Saito, Y., et al. (2021), Pre-flight Calibration and Near-Earth Commissioning Results of the Mercury Plasma Particle Experiment (MPPE) Onboard MMO (Mio), *Space Sci. Rev.*, *217*(5), 70, https://doi.org/10.1007/s11214-021-00839-2.

See, V., M. Jardine, A. A. Vidotto, P. Petit, S. C. Marsden, S. V. Jeffers, and J. D. do Nascimento (2014), The effects of stellar winds on the magnetospheres and potential habitability of exoplanets, *A&A*, *570*, A99, https://doi.org/10.1051/0004-6361/201424323.

Shay, M. A., and M. Swisdak (2004), Three-Species Collisionless Reconnection: Effect of O+ on Magnetotail Reconnection, *Physical Review Letters*, *93*(17), 175001, https://doi.org/10.1103/PhysRevLett.93.175001.

Slavin, J. A., et al. (2009), MESSENGER observations of magnetic reconnection in Mercury's magnetosphere, *Science*, *324*(5927), 606-610, https://doi.org/10.1126/science.1172011.

Slavin, J. A., et al. (2010), MESSENGER observations of extreme loading and unloading of Mercury's magnetic tail, *Science*, *329*(5992), 665-668, https://doi.org/10.1126/science.1188067.

Slavin, J. A., et al. (2012), MESSENGER and Mariner 10 flyby observations of magnetotail structure and dynamics at Mercury, *J. Geophys. Res. Space Physics*, *117*(A1), A01215, https://doi.org/10.1029/2011ja016900.

Slavin, J. A., and R. E. Holzer (1979), The effect of erosion on the solar wind stand-off distance at Mercury, *J. Geophys. Res. Space Physics*, *84*(A5), 2076-2082, https://doi.org/10.1029/JA084iA05p02076.

Slavin, J. A., S. M. Imber, and J. M. Raines (2021), *A Dungey Cycle in the Life of Mercury's Magnetosphere*, American Geophysical Union, Magnetospheres in the Solar System.

Slavin, J. A., et al. (2019), MESSENGER Observations of Disappearing Dayside Magnetosphere Events at Mercury, *J. Geophys. Res. Space Physics*, *124*(8), 6613-6635, https://doi.org/10.1029/2019ja026892.

Slavin, J. A., E. I. Tanskanen, M. Hesse, C. J. Owen, M. W. Dunlop, S. Imber, E. A. Lucek, A. Balogh, and K.-H. Glassmeier (2005), Cluster observations of traveling compression regions in the near-tail, *Journal of Geophysical Research: Space Physics*, *110*(A6), https://doi.org/https://doi.org/10.1029/2004JA010878.

Smith, A. W., C. M. Jackman, C. M. Frohmaier, J. C. Coxon, J. A. Slavin, and R. C. Fear (2018), Evaluating Single-Spacecraft Observations of Planetary Magnetotails With Simple Monte Carlo Simulations: 1. Spatial Distributions of the Neutral Line, *J. Geophys. Res. Space Physics*, *123*(12), 10,109-110,123, https://doi.org/10.1029/2018ja025958.

Smith, A. W., J. A. Slavin, C. M. Jackman, G. K. Poh, and R. C. Fear (2017), Flux ropes in the Hermean magnetotail: Distribution, properties, and formation, *J. Geophys. Res. Space Physics*, *122*(8), 8136-8153, https://doi.org/10.1002/2017JA024295.

Sonnerup, B. U. O. (1979), Magnetic field reconnection, *in Solar System Plasma Physics III, edited by L. J. Lanzerotti, C. F. Kennel, and E. N. Parker*, 45-108.

Sonnerup, B. U. Ö. (1974), Magnetopause reconnection rate, *Journal of Geophysical Research (1896-1977)*, *79*(10), 1546-1549, https://doi.org/https://doi.org/10.1029/JA079i010p01546.

Sonnerup, B. U. Ö., and M. Scheible (1998), Minimum and maximum variance analysis, in Analysis Methods for Multi-Spacecraft Data, edited by G. Paschmann and P. W. Daly, *Int. Space Sci. Inst., Bern, Switzerland.*, 185-220.

Sun, W. J., S. Y. Fu, J. A. Slavin, J. M. Raines, Q. G. Zong, G. K. Poh, and T. H. Zurbuchen (2016), Spatial distribution of Mercury's flux ropes and reconnection fronts: MESSENGER observations, *J. Geophys. Res. Space Physics*, *121*(8), 7590-7607, https://doi.org/10.1002/2016JA022787.

Sun, W. J., J. A. Slavin, R. M. Dewey, Y. Chen, G. A. DiBraccio, J. M. Raines, J. M. Jasinski, X. Jia, and M. Akhavan-Tafti (2020a), MESSENGER Observations of Mercury's Nightside Magnetosphere Under Extreme Solar Wind Conditions: Reconnection-Generated Structures and Steady Convection, *J. Geophys. Res. Space Physics*, *125*(3), e2019JA027490, https://doi.org/10.1029/2019ja027490.

Sun, W. J., et al. (2020b), Flux Transfer Event Showers at Mercury: Dependence on Plasma β and Magnetic Shear and Their Contribution to the Dungey Cycle, *Geophy. Res. Lett.*, *47*(21), e2020GL089784, https://doi.org/https://doi.org/10.1029/2020GL089784.

Winslow, R. M., B. J. Anderson, C. L. Johnson, J. A. Slavin, H. Korth, M. E. Purucker, D. N. Baker, and S. C. Solomon (2013), Mercury's magnetopause and bow shock from MESSENGER Magnetometer observations, *J. Geophys. Res. Space Physics*, *118*, 2213-2227, https://doi.org/10.1002/jgra.50237.

Winslow, R. M., et al. (2014), Mercury's surface magnetic field determined from proton-reflection magnetometry, *Geophy. Res. Lett.*, *41*(13), 4463-4470, https://doi.org/doi:10.1002/2014GL060258.

Zhao, J.-T., Q.-G. Zong, J. A. Slavin, W.-J. Sun, X.-Z. Zhou, C. Yue, J. M. Raines, and W.-H. Ip (2020), Proton Properties in Mercury's Magnetotail: A Statistical Study, *Geophy. Res. Lett.*, *47*(19), e2020GL088075, https://doi.org/10.1029/2020gl088075.

Zhong, J., L. C. Lee, X. G. Wang, Z. Y. Pu, J. S. He, Y. Wei, and W. X. Wan (2020a), Multiple X-line Reconnection Observed in Mercury's Magnetotail Driven by an Interplanetary Coronal Mass Ejection, *Astrophys. J. Lett.*, *893*(1), L11, https://doi.org/10.3847/2041-8213/ab8380.

Zhong, J., W. X. Wan, J. A. Slavin, Y. Wei, R. L. Lin, L. H. Chai, J. M. Raines, Z. J. Rong, and X. H. Han (2015), Mercury's three-dimensional asymmetric magnetopause, *J. Geophy. Res. Space Physics*, *120*, 7658-7671, https://doi.org/10.1002/2015JA021425.

Zhong, J., Y. Wei, L. C. Lee, J. S. He, J. A. Slavin, Z. Y. Pu, H. Zhang, X. G. Wang, and W. X. Wan (2020b), Formation of Macroscale Flux Transfer Events at Mercury, *Astrophys. J. Lett.*, *893*(1), L18, https://doi.org/10.3847/2041-8213/ab8566.

Zhong, J., et al. (2018), MESSENGER Observations of Rapid and Impulsive Magnetic Reconnection in Mercury's Magnetotail, *Astrophys. J. Lett.*, *860*(2), L20, https://doi.org/10.3847/2041-8213/aaca92.

List of active magnetic reconnection events observed by the MESSENGER spacecraft.

Column 1: Orbit number.

Column 2: Time interval for the data analysis, or identified Hall region.

Column 3-6: Current sheet location in solar wind-aberrated Mercury solar magnetospheric (aMSM) coordinate and magnetic local time.

Column 7-9: Local current sheet coordinate system (LMN).

Column 10: guide field.

Column 11-14: Observed Hall magnetic field quadrants (1: observed; 0: not observed or unclear).

Column 15: Identified reconnection event type. Case 1: crossing the planetward side of the X-lines; Case 2: crossing of X-lines region; Case 3: crossing the tailward side of the X-lines.

		Current sheet location				Local current sheet coordinates				Observed Hall field quadrants				
orbit	Time interval	X	Y	Z	LMT	L	M	N	Bguide (nT)	I	II	III	IV	Case type
0321	2011-08-25/08:10:45-08:17:40	-2.87	-0.34	-0.26	0.447	(0.991, 0.094, 0.097)	(-0.094, 0.996, 0.000)	(-0.097,-0.009, 0.995)	5.5	1	0	1	1	2
0338	2011-09-02/20:21:58-20:30:37	-1.98	1.47	0.17	21.557	(0.987,-0.140,-0.076)	(0.140, 0.990, 0.000)	(0.075,-0.011, 0.997)	-3.1	1	0	1	0	1
0486	2011-11-14/21:27:05-21:33:21	-2.02	-1.34	0.04	2.230	(0.991, 0.136,-0.012)	(-0.136, 0.991, 0.000)	(0.012, 0.002, 1.000)	2.9	1	1	0	1	2
0496	2011-11-19/21:23:54-21:27:49	-2.52	-0.57	-0.11	0.844	(0.993, 0.082, 0.083)	(-0.082, 0.997, 0.000)	(-0.083,-0.007, 0.997)	5.8	1	1	0	0	2
0498	2011-11-20/21:21:23-21:28:14	-2.62	-0.37	-0.16	0.537	(0.998, 0.024, 0.065)	(-0.024, 1.000, 0.000)	(-0.065,-0.002, 0.998)	7.4	1	1	1	1	2
0503	2011-11-23/09:22:41-09:28:02	-2.60	0.17	-0.12	23.758	(0.998,-0.048, 0.049)	(0.048, 0.999, 0.000)	(-0.049, 0.002, 0.999)	27.1	0	1	0	1	3
0681	2012-02-19/00:43:47-00:47:31	-2.32	0.11	-0.00	23.822	(0.994, 0.051, 0.093)	(-0.052, 0.999, 0.000)	(-0.092,-0.005, 0.996)	-7.7	1	1	1	1	2
0695	2012-02-25/21:48:32-21:51:30	-1.71	1.39	0.12	21.383	(0.988,-0.152,-0.009)	(0.152, 0.988, 0.000)	(0.009,-0.001, 1.000)	-1.3	1	0	1	0	1
0877	2012-05-12/22:34:37-22:35:12	-2.05	-0.54	-0.12	0.978	(0.954, 0.289, 0.074)	(-0.290, 0.957,-0.000)	(-0.070,-0.021, 0.997)	-1.2	0	1	0	1	3
0890	2012-05-17/06:34:55-06:36:09	-2.13	0.19	-0.14	23.652	(0.991, 0.037, 0.125)	(-0.037, 0.999, 0.000)	(-0.125,-0.005, 0.992)	-4.4	1	1	1	1	2
0892	2012-05-17/22:30:45-22:35:26	-2.16	0.33	-0.21	23.420	(0.980,-0.005, 0.197)	(0.005, 1.000, 0.000)	(-0.197, 0.001, 0.980)	2.7	1	1	1	1	2
0896	2012-05-19/06:32:32-06:37:17	-2.08	0.57	-0.17	22.972	(0.977, 0.017, 0.213)	(-0.017, 1.000, 0.000)	(-0.213,-0.004, 0.977)	-2.4	1	1	0	1	2
0897	2012-05-19/14:34:08-14:40:05	-2.04	0.63	-0.14	22.861	(0.995, 0.060, 0.081)	(-0.060, 0.998, 0.000)	(-0.081,-0.005, 0.997)	-1.6	1	0	1	0	1
1164	2012-08-16/14:56:20-14:58:30	-1.76	0.74	0.06	22.482	(0.998,-0.041, 0.039)	(0.041, 0.999,-0.000)	(-0.039, 0.002, 0.999)	4.4	1	1	1	1	2
1681	2013-02-04/23:37:10-23:39:46	-1.78	0.18	0.05	23.613	(0.997, 0.024, 0.076)	(-0.024, 1.000,-0.000)	(-0.076,-0.002, 0.997)	11.6	1	0	1	0	1
1948	2013-05-05/00:04:33-00:07:45	-1.64	0.33	0.09	23.232	(0.995,-0.092, 0.022)	(0.092, 0.996, 0.000)	(-0.022, 0.002, 1.000)	-6.9	1	0	1	0	1
2553	2013-11-22/18:06:19-18:08:46	-2.02	-0.62	-0.15	1.138	(0.952, 0.305, 0.009)	(-0.305, 0.952, 0.000)	(-0.009,-0.003, 1.000)	-2.4	1	0	1	0	1
2574	2013-11-29/18:08:12-18:11:43	-2.04	0.46	-0.12	23.156	(0.992, 0.026, 0.125)	(-0.026, 1.000, 0.000)	(-0.125,-0.003, 0.992)	-4.8	1	0	1	0	1
2577	2013-11-30/18:06:43-18:08:51	-1.94	0.58	-0.04	22.888	(0.998, 0.024, 0.052)	(-0.024, 1.000, 0.000)	(-0.052,-0.001, 0.999)	2.8	1	0	1	0	1
2578	2013-12-01/02:05:17-02:08:50	-1.90	0.62	-0.01	22.799	(1.000,-0.031,-0.005)	(0.031, 1.000,-0.000)	(0.005,-0.000, 1.000)	3.1	1	0	1	0	1
2809	2014-02-16/02:33:40-02:38:12	-1.76	-0.96	0.04	1.900	(0.972, 0.232, 0.034)	(-0.232, 0.973,-0.000)	(-0.033,-0.008, 0.999)	-3.4	1	1	1	1	2
2829	2014-02-22/18:33:58-18:38:59	-1.90	0.09	0.15	23.828	(0.980, 0.197,-0.005)	(-0.197, 0.980,-0.000)	(0.005, 0.001, 1.000)	8.8	1	0	1	0	1
2832	2014-02-23/18:36:35-18:39:25	-1.94	0.22	0.10	23.567	(0.986, 0.151,-0.072)	(-0.151, 0.988, 0.000)	(0.072, 0.011, 0.997)	4.7	1	0	1	0	1
2840	2014-02-26/10:39:49-10:42:06	-1.95	0.58	0.01	22.893	(0.996, 0.089,-0.025)	(-0.089, 0.996, 0.000)	(0.025, 0.002, 1.000)	0.5	1	0	1	0	1
2849	2014-03-01/10:42:15-10:46:53	-1.90	0.97	-0.11	22.195	(0.954,-0.234, 0.187)	(0.238, 0.971, 0.000)	(-0.182, 0.045, 0.982)	0.6	1	0	1	0	1
3072	2014-05-14/19:19:36-19:23:35	-2.04	-1.18	-0.32	2.005	(0.948, 0.285, 0.140)	(-0.287, 0.958,-0.000)	(-0.134,-0.040, 0.990)	-6.0	1	1	1	1	2
3073	2014-05-15/03:18:41-03:23:30	-2.04	-1.10	-0.27	1.883	(0.936, 0.255, 0.244)	(-0.263, 0.965, 0.000)	(-0.235,-0.064, 0.970)	-2.1	1	0	1	0	1
3079	2014-05-17/03:11:19-03:16:42	-1.86	-0.58	0.14	1.144	(0.977, 0.178,-0.113)	(-0.179, 0.984, 0.000)	(0.112, 0.020, 0.994)	7.9	1	1	1	1	2
3086	2014-05-19/11:15:33-11:17:07	-2.03	-0.24	0.05	0.449	(0.946, 0.198,-0.256)	(-0.205, 0.979, 0.000)	(0.251, 0.053, 0.967)	3.6	1	1	0	1	2
3339	2014-08-12/01:11:49-01:15:56	-1.88	-0.74	0.14	1.429	(0.899, 0.430,-0.080)	(-0.431, 0.902, 0.000)	(0.072, 0.034, 0.997)	10.6	1	0	1	0	1
3350	2014-08-15/17:35:47-17:39:15	-2.05	-0.16	0.10	0.291	(0.975, 0.210,-0.071)	(-0.211, 0.978, 0.000)	(0.069, 0.015, 0.997)	9.6	1	0	1	0	1
3351	2014-08-16/01:37:51-01:41:07	-2.17	-0.12	-0.02	0.219	(0.955, 0.292,-0.043)	(-0.292, 0.956,-0.000)	(0.042, 0.013, 0.999)	9.1	1	0	1	0	1
3352	2014-08-16/09:39:05-09:43:33	-2.03	-0.05	0.12	0.091	(0.991, 0.132,-0.021)	(-0.132, 0.991, 0.000)	(0.020, 0.003, 1.000)	-0.3	1	1	1	0	1
3353	2014-08-16/17:42:21-17:47:32	-2.04	0.00	0.10	23.998	(0.991, 0.123,-0.058)	(-0.123, 0.992, 0.000)	(0.058, 0.007, 0.998)	12.1	1	0	1	1	2
3375	2014-08-24/02:27:09-02:32:53	-1.85	1.00	0.05	22.111	(0.975,-0.216, 0.058)	(0.217, 0.976,-0.000)	(-0.056, 0.012, 0.998)	1.6	1	0	1	0	1
3378	2014-08-25/02:37:26-02:40:43	-1.84	1.14	-0.02	21.891	(0.957,-0.269, 0.107)	(0.271, 0.963, 0.000)	(-0.103, 0.029, 0.994)	6.3	1	0	1	0	1
3602	2014-11-08/17:08:18-17:12:39	-2.48	-0.82	-0.31	1.226	(0.983, 0.093, 0.160)	(-0.095, 0.996,-0.000)	(-0.159,-0.015, 0.987)	-10.2	1	1	0	1	3
3604	2014-11-09/09:30:21-09:37:41	-2.49	-0.67	-0.27	1.002	(0.989,-0.043, 0.143)	(0.043, 0.999, 0.000)	(-0.142, 0.006, 0.990)	3.6	0	1	1	1	3
3608	2014-11-10/18:19:28-18:26:46	-2.53	-0.39	-0.25	0.576	(0.988, 0.013, 0.156)	(-0.013, 1.000, 0.000)	(-0.156,-0.002, 0.988)	5.4	1	1	0	1	2
3618	2014-11-14/04:27:20-04:30:34	-2.43	0.27	-0.12	23.572	(0.998,-0.016, 0.053)	(0.016, 1.000, 0.000)	(-0.053, 0.001, 0.999)	-0.8	1	1	1	1	2
3630	2014-11-18/07:05:03-07:07:52	-2.43	0.97	-0.32	22.544	(0.975,-0.167, 0.145)	(0.168, 0.986, 0.000)	(-0.143, 0.024, 0.989)	1.0	0	1	0	1	3
3855	2015-02-03/09:17:43-09:22:18	-2.28	-0.98	-0.06	1.549	(0.977, 0.212, 0.021)	(-0.212, 0.977, 0.000)	(-0.020,-0.004, 1.000)	-4.3	1	1	1	1	2
3858	2015-02-04/10:01:08-10:10:01	-2.26	-0.73	0.04	1.190	(0.971, 0.234,-0.054)	(-0.234, 0.972, 0.000)	(0.053, 0.013, 0.999)	-4.5	1	0	1	0	1

3865	2015-02-06/19:55:30-20:05:04	-2.32	-0.26	0.07	0.426	(0.990, 0.017,-0.138)	(-0.017, 1.000, 0.000)	(0.138, 0.002, 0.990)	-1.8	1	1	1	1	2
3872	2015-02-09/05:51:26-05:58:12	-2.18	0.17	0.20	23.694	(0.993,-0.104,-0.052)	(0.104, 0.995, 0.000)	(0.052,-0.005, 0.999)	-8.5	1	0	1	0	1
3874	2015-02-09/22:29:36-22:32:18	-2.30	0.29	0.08	23.529	(0.998, 0.060, 0.002)	(-0.060, 0.998, 0.000)	(-0.002,-0.000, 1.000)	5.9	1	1	1	0	2
3877	2015-02-10/23:16:13-23:19:40	-2.15	0.44	0.19	23.224	(0.994,-0.046,-0.104)	(0.046, 0.999, 0.000)	(0.104,-0.005, 0.995)	-0.5	1	0	1	0	1
3888	2015-02-14/18:16:35-18:21:36	-1.97	0.97	0.18	22.261	(0.989,-0.141,-0.047)	(0.141, 0.990,-0.000)	(0.047,-0.007, 0.999)	2.5	1	0	1	0	1
3889	2015-02-15/02:37:38-02:41:57	-2.10	1.06	0.04	22.209	(0.971,-0.237, 0.023)	(0.238, 0.971, 0.000)	(-0.022, 0.005, 1.000)	-8.5	1	0	1	0	1
3890	2015-02-15/10:50:32-10:54:40	-1.93	1.05	0.19	22.095	(0.991,-0.127,-0.042)	(0.127, 0.992, 0.000)	(0.042,-0.005, 0.999)	3.3	1	0	1	0	1
3895	2015-02-17/04:20:37-04:23:27	-2.05	1.37	-0.06	21.745	(0.967,-0.254, 0.036)	(0.254, 0.967,-0.000)	(-0.035, 0.009, 0.999)	-1.5	1	0	1	0	1